(NASA-CR-161551) SPECTRUM SYNTHESIS OF EUV SOLAR FLARE LINE PROFILES Final Report (Weber State Coll.) 18 p HC A02/MF A01 CSCL 03B
N80-32315
Unclas
G3/92 28591

1. Introduction:

On June 15, 1973, a classic double ribbon flare of importance 1B occurred at approximately 1405 UT, reaching an H-α maximum at 1413 UT, and ended at 1455 UT. The flare occurred in an old and simplifying bipolar region at N18 W32. Of all the 18 flares and sub-flares observed during the Skylab missions, this flare has received the greatest amount of attention with over a dozen publications covering various aspects of the event, (e.g. see Widing and Dere (1977)). An H-α photograph of this event is shown in Fig. 1.

The author chose this flare to study because of the extensive temporal data available. A total of 136 spectra of wavelength ranges from 1100 to 3000 Å were taken during the flare's duration by the Naval Research Laboratory (NRL) normal incidence slit spectrograph (SO 82-B).

The purpose of this research was to determine, using the aforementioned spectral data, the nature of the solar chromosphere of a flare event as a function of time.

2. Experimental Results of Flare Observations:

A total of 77 spectral line profiles at λ1206 due to Si-III and λ1265, λ1522, and λ1816 due to Si-II were selected from the data. A montage of the relative intensity of some of these line profiles at various times is shown in Fig.2. Two components of the portion of the flare emitting within the field of view were observed: a stationary component and a moving component. The latter component was seen during the first two minutes of observations of what is called the eruptive phase.

The relative intensities of these spectral line profiles were converted to absolute intensities using the calibration of Feldman, et al (1976). The peak line of intensity of the stationary component as a function of time is summarized in Fig. 3 along with the Solrad 0-3 Å X-ray flux, the H-α flux, and the Fe XXI relative intensity. Although the temporal resolution of the EUV spectral data is far from optimum, Fig. 3 shows the Si-II and Si-III spectral lines reaching an apparent maximum during the eruptive phase by as much as 30 sec prior to the H-α and the soft X-ray maxima and some 1.5 min after the 2.7-5.0 GHz microwave burst.

Tripp, et al (1976) indicated from spectrum synthesis of these same EUV spectral lines, that the line centers were formed on the average near 6500 °K for λ1816, 7500 °K for λ1533, 8600 °K for λ1265, and 20,000 °K for λ1206. Thus these Si-II resonance lines are formed mainly on the middle-chromosphere temperature plateau and the Si-III resonance line in the upper-chromosphere temperature plateau.

It is currently believed that the site of the primary flare energy release is in the corona (Canfield 1980). If this view is correct, then the flare phenomena occuring lower in the solar atmosphere must be the result of transfer of energy downward from the release site in the corona.

However, the data summarized in Fig. 3 tends not to support this view, but shows this disturbance to be deeper in the solar atmosphere. Because the temporal resolution is not particular good, it is impossible to follow the flare disturbance up through the atmosphere using these four spectral lines, which correspond to different altitudes in the solar atmosphere. However, the second increase in intensity corresponding to the main phase of the flares, which occurs on a much slower time scale, indicates that this increase in intensity begins with the λ1816 line and ends with the λ1206 line as though the disturbance is still propagating upward. Thus the data tend to indicate that back warming from the corona above may not be a substantial phenomena for this flare. The variation in the Fe XXI intensity, which is obviously formed at peak temperatures, occurs some time after the eruptive phase.

One may conclude from the data; therefore, that the flare energy release occurs low in the solar atmosphere and somehow builds to maximum in the corona. It would appear that perhaps some sort of shock wave may be involved in the energy transport process. This result tends to substantiate the findings of Machado and Linsky (1975).

As mentioned above, the flare of June 15, 1973 is a double ribbon flare. As can be seen in Fig. 1, the slit of the spectrometer is across one of the ribbons. Since a pre-disperser is used on the spectrograph, all spatial resolution along the length of the slit was lost.

Some of the line profiles in Fig. 2 indicate the presence of the ribbon material. Asymmetries in three of the four spectral lines near their flare maxima indicate blue shifts corresponding to this ejected material. Line profiles for the ribbon have been de-convolved with the main flare profile and are shown in Fig. 4. These data indicate shown upward movement of the ribbon averaging approximately 50-75 Kms^{-1}. These values are in general agreement with the findings of Feldman, et al (1977).

3. Theoretical Results:

The main thrust of this research project was to attempt modeling the chromosphere of solar flare. Attempts have been made previously by Machado and Linsky (1975) of the photosphere and Lites and Cook (1979) of the transition region.

The basic technique used was to employ radiative transfer methods assuming a plane parallel, static model atmosphere in hydrostatic equilibrium (HSE) in an attempt to synthesize these same four silicon lines. Comparing the fit to the spectral data then acted as a means of determining the validity of the model atmosphere.

The method of calculation used a version of the complete linearization technique of Auer and Mihalas (1969). Complete redistribution was used. Arguments for such an approach are found in Tripp, et al (1976).

The synthetic spectrum calculations were carried out on the CDC 7600 computer located at the National Center for Atmospheric Research (NCAR) located in Boulder, Colorado.

Over twenty-five trial model atmospheres were attempted using the atmospheres of Machado, Emslie, and Brown (1978) and Lites and Cook (1979) as a starting point. It was found that essentially a separate model atmosphere was needed for each line in order to get a reasonable intensity fit. The four temperature models are shown in Fig. 5 along with the Machado, Emslie and Brown (M-E-B) and Lites and Cook (L-C) models. This finding seems reasonable since each line is formed at a different height, and the temperature distribution is dynamic in nature. Model atmosphere No. 19 seemed to give the best intensity fit to the λ1816 line, No. 20 to the λ1533 line, No. 21 to the λ1265 line, and No. 22 to the λ1206 line. The computed line profiles for these cases are shown in Fig. 6.

The various temperature models mentioned above show that the physical extent of the chromosphere appears to get smaller with time. It should be pointed out that the shape of the chromospheric temperature distribution tends to substantiate the experimental finding mentioned above. The general shape seems to indicate a warming from below. The amount of heating seems to increase with height in comparison to the VAL model atmosphere plotted in the same figure.

The coronal overburdens, or the mass column density above the level where the Lyman-continuum optical depth is unity, for the cases 19, 20, 21, and 22 were 0.0 $g \cdot cm^{-2}$, 1.0×10^{-8} $g \cdot cm^{-2}$, 1.0×10^{-5} $g \cdot cm^{-2}$, and 1.0×10^{-4} $g \cdot cm^{-2}$. These values are somewhat lower than the values used by Machado, Emslie, and Brown (1978), and is over twenty-five times greater than VAL model for the quiet sum. The author didn't use the coronal overburden as a constraint on the model atmsophere simply because at the times being treated in the spectrum synthesis, the Lyman continuum was not at maximum intensity.

The models suffer from some computational weakness, most noticably the assumption of hydrostatic equilibrium. The obvious departure from HSE in a solar flare makes our models a first-order estimate at best. For this reason we have not pressed our calculations to fit in detail the experimental data.

The derived electron densities were typically found to be 10^{10} to 10^{11} electrons$\cdot cm^{-3}$ in the chromosphere. These values are an order of magnitude or so lower than those quoted by Lites and Cook (1979). However, again our modeling occurred at times prior to the main phase. It would seem reasonable; therefore, that the electron densities be less.

The non-thermal velocity distribution appears from our calculations to follow that of Lites and Cook (1979) peaking at 20 $Km \cdot s^{-1}$ in the transition region.

4. <u>Summary</u>:

In conclusion, both the experimental and theoretical data tend to show that the flare of June 15, 1973 did not have its beginnings in the corona, but low in the solar atmosphere.

The work performed under this grant would tend to point out the need for flare data with better time resolution. Also if per-flare data were available, the plage region could be empirically modeled prior to flaring, thus allowing the abandonment of the hydrostatic equilibrium constraint used in this flare modeling work.

Hopefully, these inadequacies can be remedied during the Solar Maximum Mission.

BIBLIOGRAPHY

Auer, L. H., and Mihalas, D., 1969, Astrophys J. 158, 641.

Canfield, R. C., 1980, Solar Flares ed. P. Sturrock (Colorado Associated University Press) p. 231.

Feldman, U., Doschel, G. A., Van Hoosier, M. E., and Purcell, J. O., 1976, Astrophys. J. Suppl Series, 31, 445.

Feldman, U., Doschek, G. A., and Rosenberg, R.D.m 1977, Astrophys. J., 215, 652.

Lites, B. W., and Cook, J. W., 1979, Astrophys. J., 228, 598.

Machado, M. E., and Linskie, I. L., 1975, Solar Phys., 42, 395.

Machado, M. E., Emslie, A. G., and Brown, J. C., 1978, Solar Phys., 58, 363.

Tripp, D. A., Athay, R. G., Peterson, V. L., 1976, Astrophys. J., 220, 314.

Widing, K. G., and Dere, K. P., 1977, Solar Phys., 55, 431.

APPENDIX

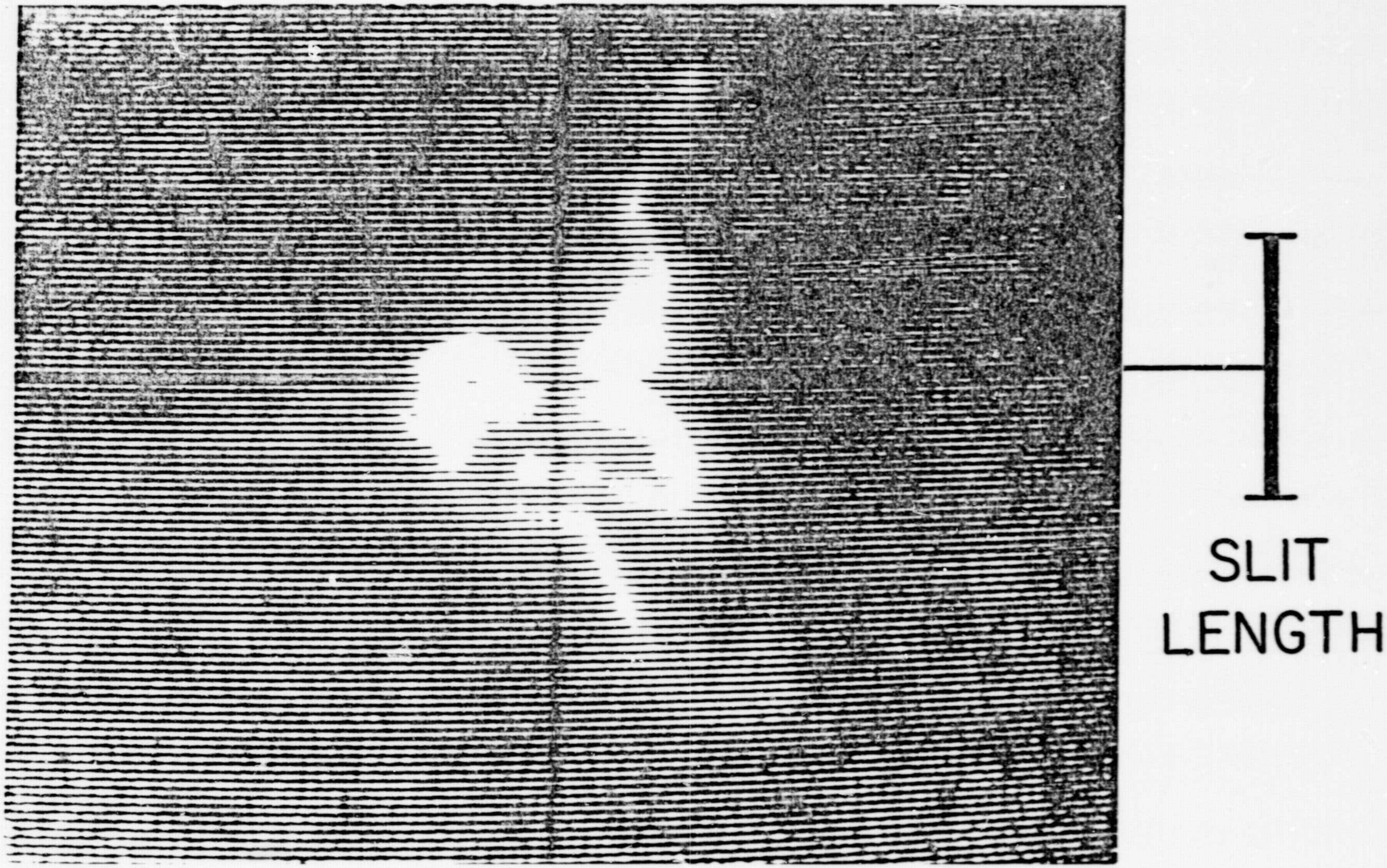

FLARE, JUNE 15th 1973

Fig. 1

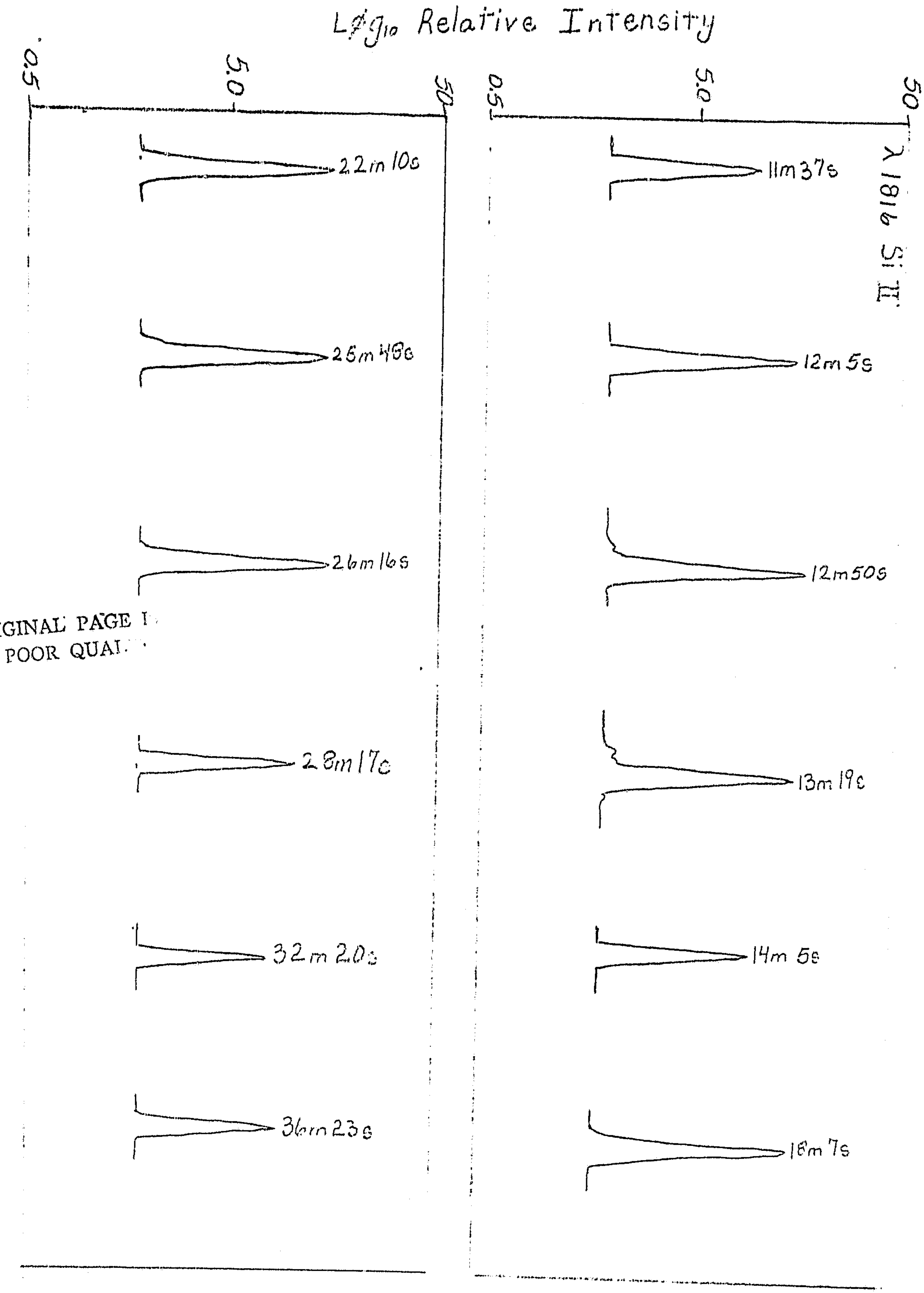

Log10 Relative Intensity
0.5
5.0
50
22m 10s
25m 48s
26m 16s
28m 17s
32m 20s
36m 23s
0.5
5.0
50
λ 1816 Si II
11m 37s
12m 5s
12m 50s
13m 19s
14m 5s
18m 7s

Fig. 2(a)

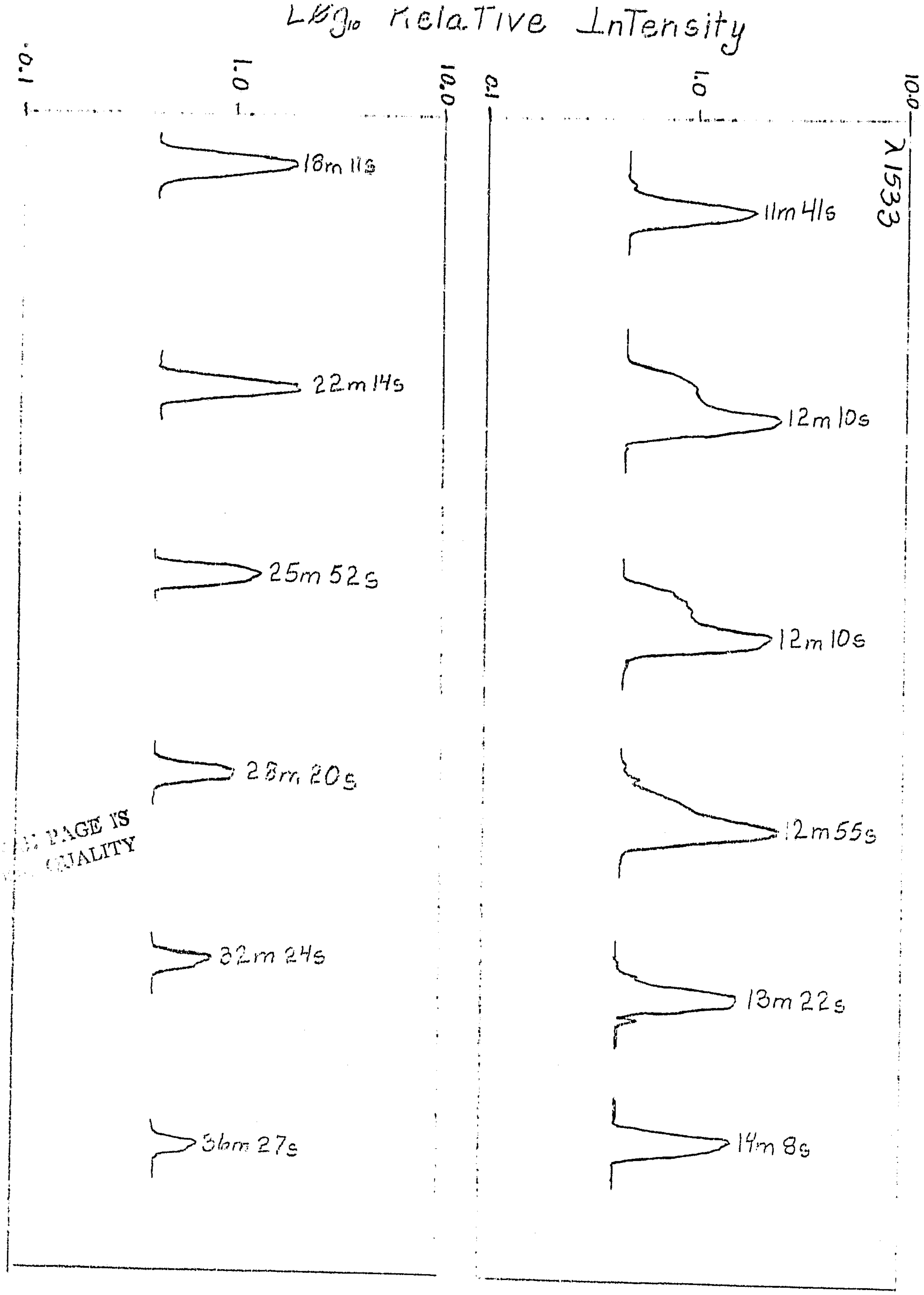
Log10 Relative Intensity
0.1
1.0
10.0
0.1
1.0
10.0
λ1533
18m 11s
22m 14s
25m 52s
28m 20s
32m 24s
36m 27s
11m 41s
12m 10s
12m 10s
12m 55s
13m 22s
14m 8s

Fig. 2(b)

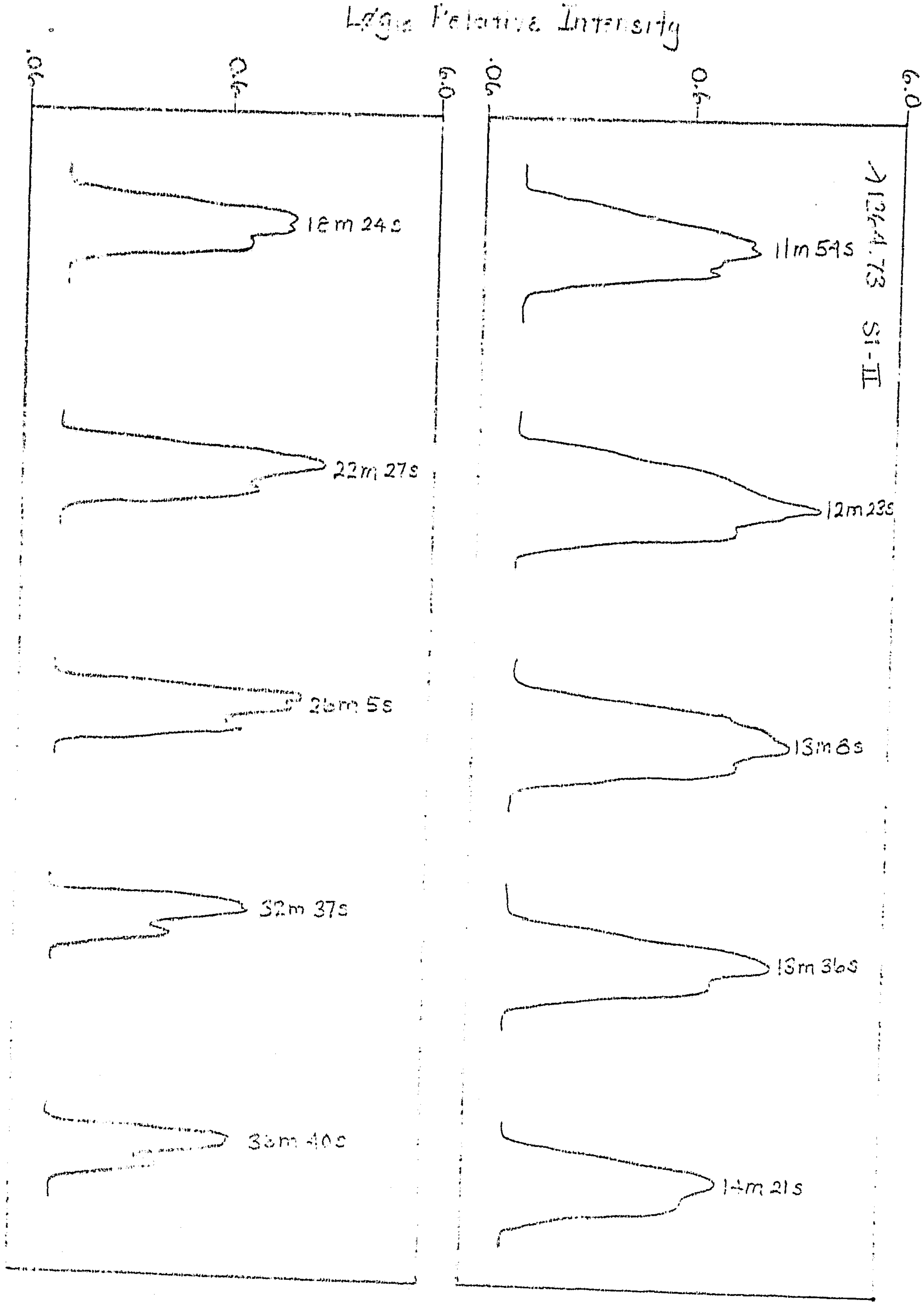
Log Relative Intensity
18m 24s
22m 27s
32m 37s
11m 59s
12m 23s
13m 6s
14m 21s

Fig. 2(c)

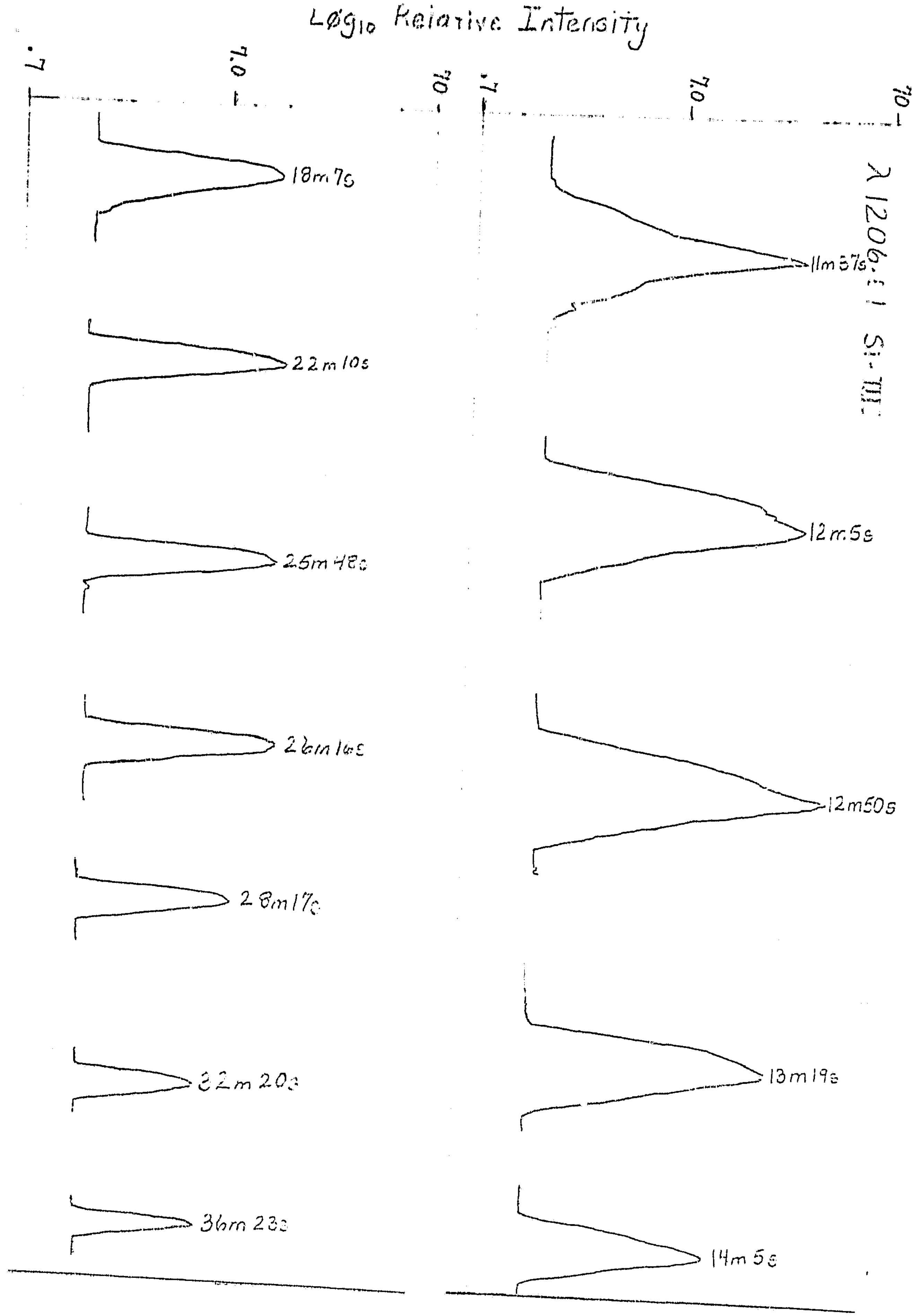
Log10 Relative Intensity
λ1206.51 Si-III
.7
7.0
70
18m7s
22m10s
25m48s
26m16s
28m17s
32m20s
36m23s
11m57s
12m5s
12m50s
13m19s
14m5s

Fig. 2(d)

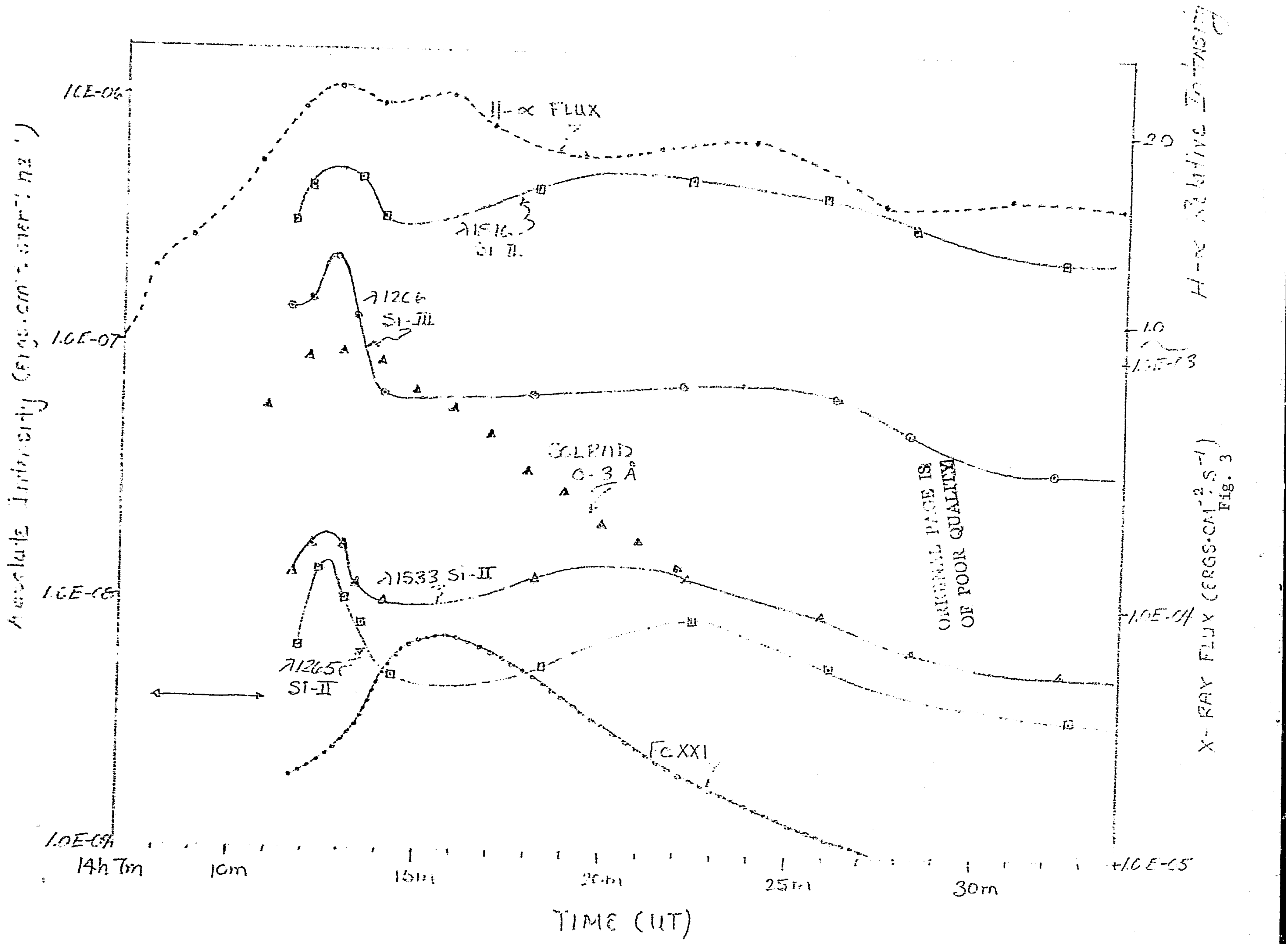

1.0E-06
1.0E-07
1.0E-08
1.0E-09
Absolute Intensity (ergs·cm⁻²·s⁻¹)
H-α FLUX
λ1816 Si II
λ1206 Si-III
SOLRAD 0-3 Å
λ1533 Si-II
λ1265 Si-II
Fe XXI
2.0
1.0
1.0E-03
1.0E-04
1.0E-05
H-α Relative Intensity
X-RAY FLUX (ERGS·CM⁻²·S⁻¹)
14h 7m
10m
15m
20m
25m
30m
TIME (UT)

Fig. 3

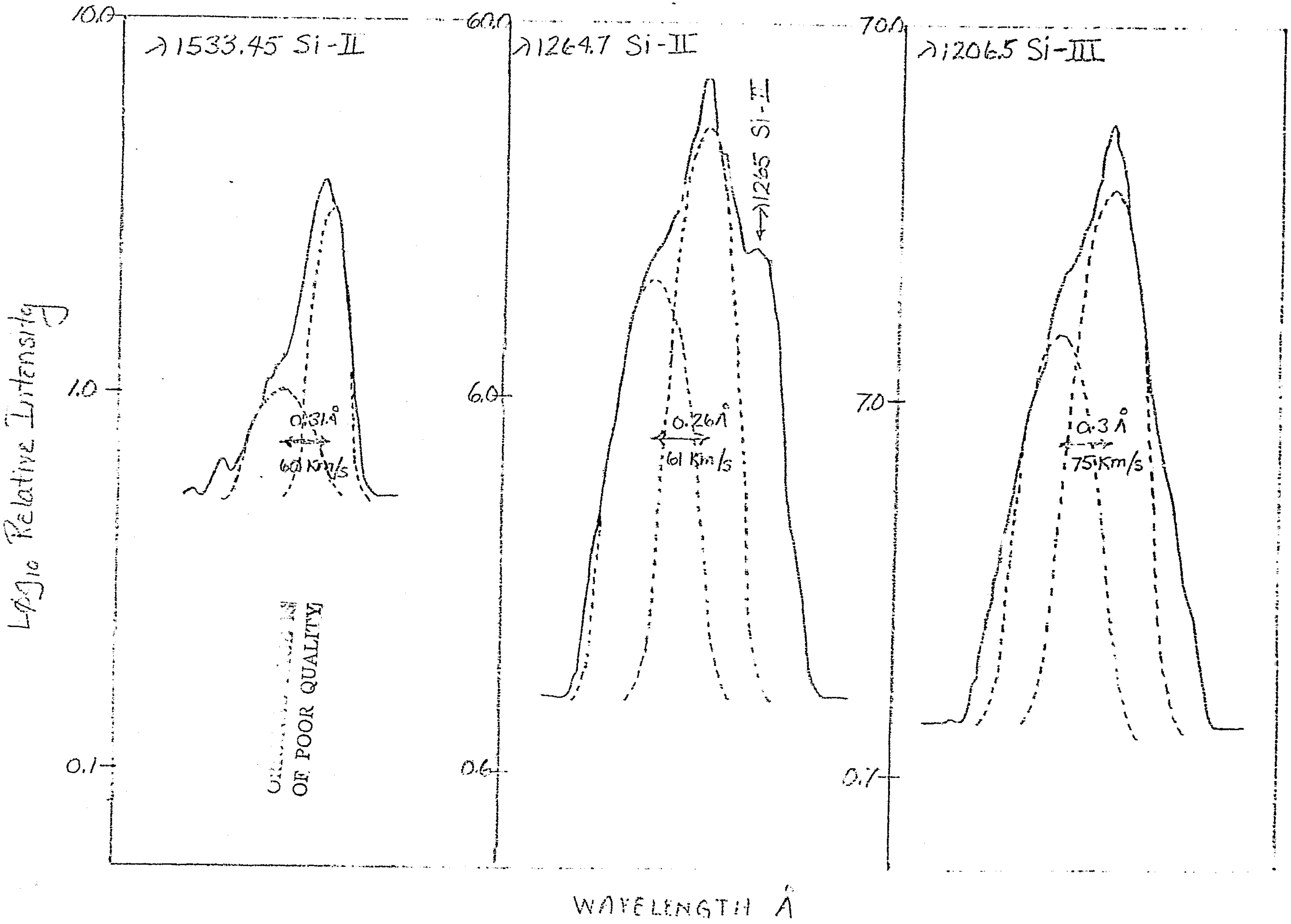

λ1533.45 Si-II
λ1264.7 Si-II
λ1206.5 Si-III
λ1265 Si-II
10.0
1.0
0.1
60.0
6.0
0.6
70.0
7.0
0.7
0.31Å
60 Km/s
0.26Å
61 Km/s
0.3 Å
75 Km/s
Log10 Relative Intensity
WAVELENGTH Å
OF POOR QUALITY

Fig. 4

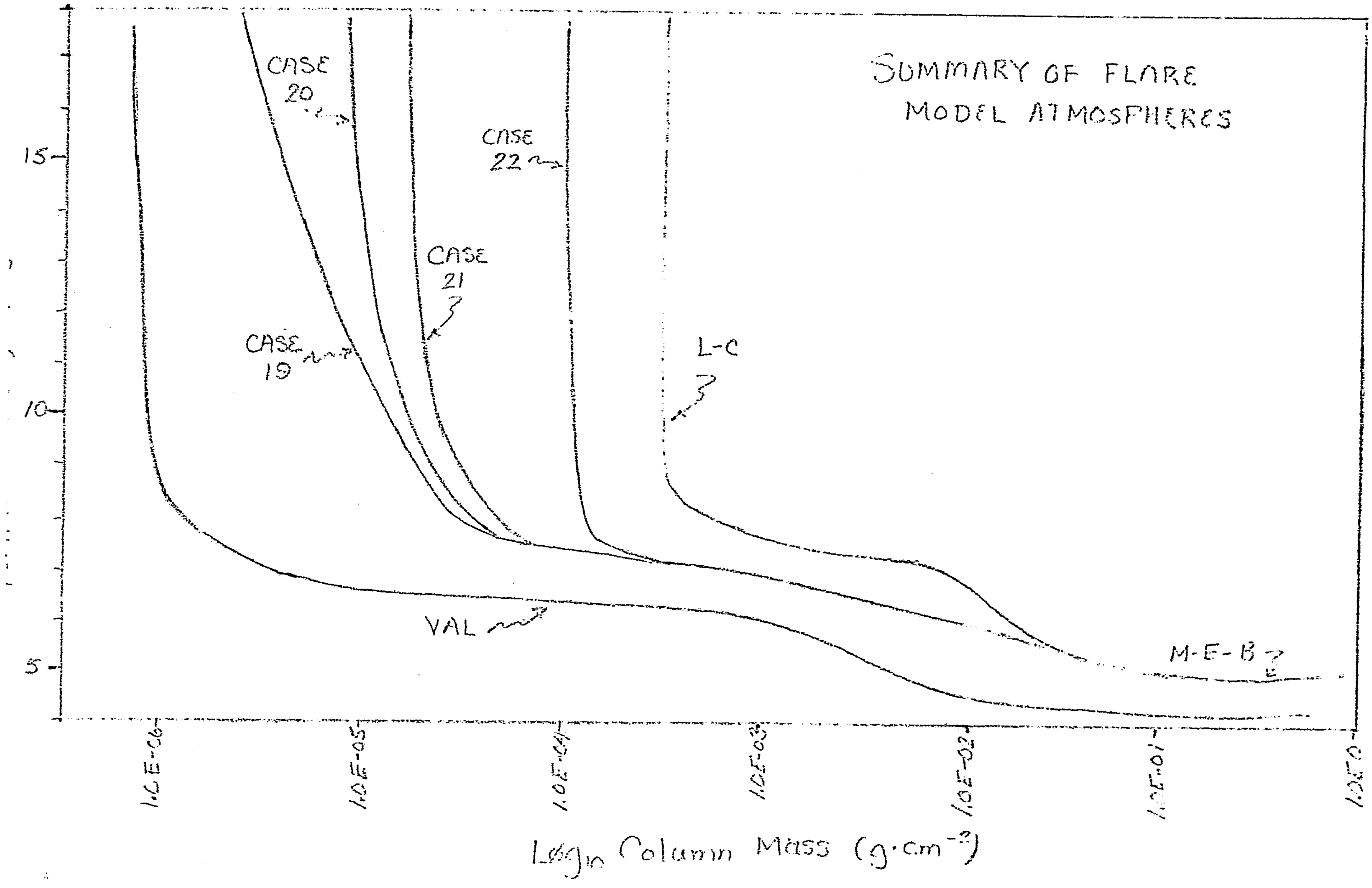
SUMMARY OF FLARE MODEL ATMOSPHERES
CASE 20
CASE 22
CASE 21
CASE 19
L-C
VAL
M-E-B
15
10
5
1.0E-06
1.0E-05
1.0E-04
1.0E-03
1.0E-02
1.0E-01
1.0E-0
Log10 Column Mass (g·cm-2)

Fig. 5

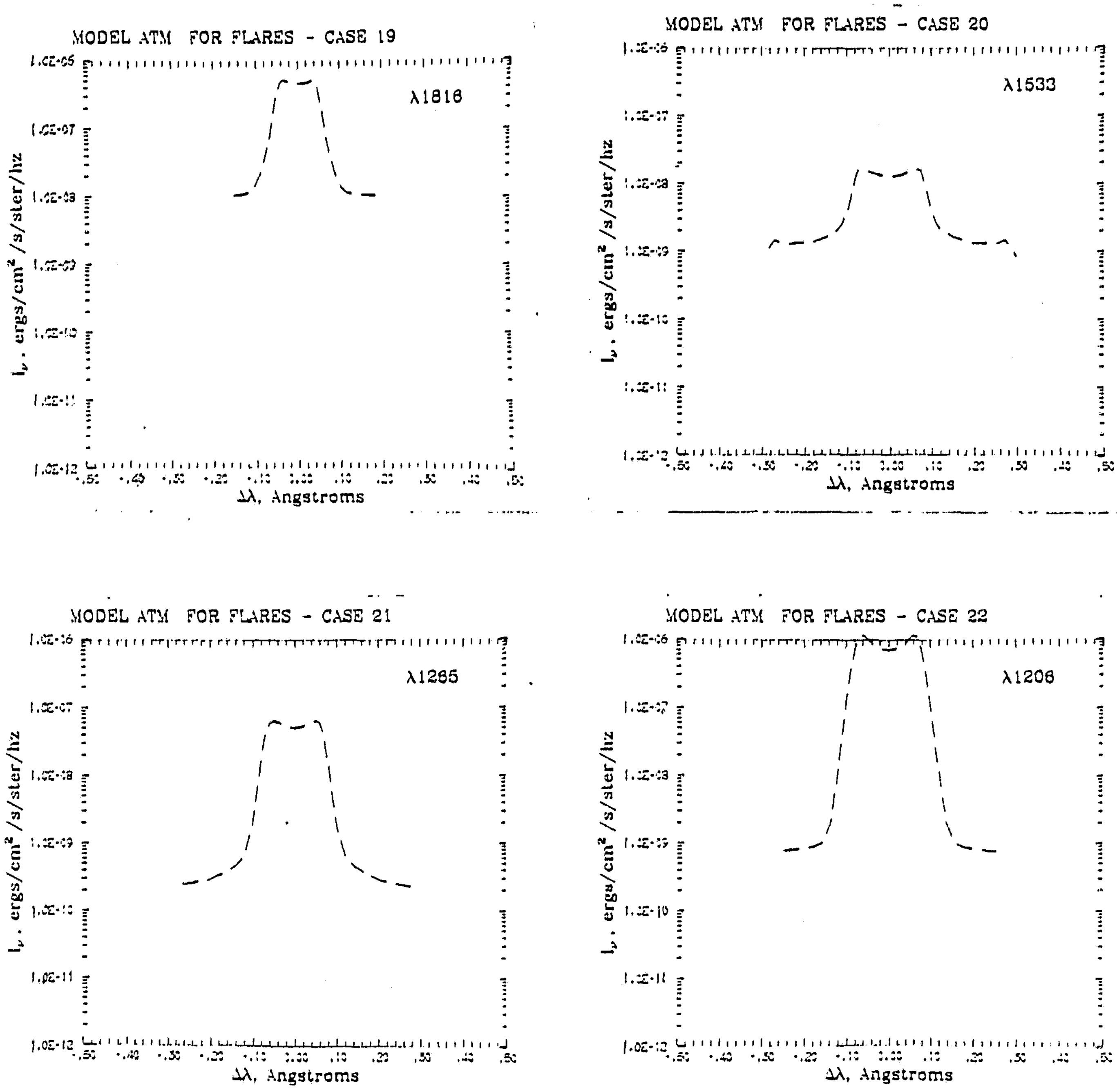
MODEL ATM FOR FLARES - CASE 19
λ1816
MODEL ATM FOR FLARES - CASE 20
λ1533
MODEL ATM FOR FLARES - CASE 21
λ1265
MODEL ATM FOR FLARES - CASE 22
λ1206
I_ν, ergs/cm^2/s/ster/hz
Δλ, Angstroms

Fig. 6